

# IMPACT OF GLOBAL NO<sub>x</sub> SOURCES ON THE NORTHERN LATITUDES

Hiram Levy II, Walter J. Moxim and Prasad S. Kasibhatla<sup>1</sup>  
Geophysical Fluid Dynamics Laboratory/NOAA  
Princeton University  
Post Box 308  
Princeton, NJ 08542  
U.S.A.

## INTRODUCTION

Nitrogen oxides (NO<sub>x</sub>), through their control of tropospheric ozone production, play a major role in determining the global reactivity of the atmosphere. The concentration of these oxides varies by as much as a factor of 1000 between continental source regions and remote locations and fluctuates significantly with season at high latitudes. While NO<sub>x</sub> levels appear to be rather low (<50 pptv) away from local sources, high levels of PAN, an important reservoir for NO<sub>x</sub>, have been measured at the surface in the winter polar regions [Barrie and Bottenheim, 1991] and in the free troposphere north of 30° N [Singh, Salas and Viezee, 1986]. Furthermore, our recent global chemical transport model (GCTM) study finds PAN to be the major reactive nitrogen species in the northern latitudes [Kasibhatla et al., 1992].

Based on a limited set of chemical measurements, primarily from the surface, it has been argued that the thermal decomposition of this sequestered PAN supplies much of the NO<sub>x</sub> in the northern latitudes, and that emissions from fossil fuel combustion are the dominant source [e.g. Barrie and Bottenheim, 1991; Honrath and Jaffe, 1992]. After checking model predictions against the available observations, we examine the hemispheric fields of NO<sub>x</sub> and PAN generated by our GCTM and quantify the contribution from fossil fuel combustion. We then determine the amount of NO<sub>x</sub> stored as PAN in the northern latitudes and compare it to direct emission from surface fossil fuel combustion and from jet aircraft.

## DESCRIPTION OF THE MODEL

We explicitly separate reactive nitrogen [NO<sub>y</sub>] into three classes of transported species; NO<sub>x</sub>, HNO<sub>3</sub>, and peroxyacetyl nitrate [PAN]. The conservation equations for their

---

<sup>1</sup>. School of Earth and Atmospheric Sciences, Georgia Institute of Technology, Atlanta, GA, 30332, USA

mixing ratios  $[R]$ ,

$$\frac{\partial}{\partial t}(R) = \textit{Advection} + \textit{Diffusion} + \textit{Filling} - \textit{Sink}_{\textit{dry}} - \textit{Sink}_{\textit{wet}} \quad (1)$$

$$+ \textit{Sources} + \textit{Chemistry},$$

are expressed in flux convergence form and integrated globally using a medium resolution (~265 km horizontal grid, 11 vertical levels) 3-D global chemical transport model (GCTM). By using the flux convergence form of (1), the global mass integral for each transported species is conserved exactly. The GCTM is driven by 6-hour time-averaged winds and a consistent total-precipitation field from the parent general circulation model (GCM) (see section 2. of Mahlman and Moxim [1978] for a summary, and Manabe et al. [1974] and Manabe and Holloway [1975] for details).

*Advection* represents tracer transport by the GCM's resolved winds. It is integrated in flux convergence form, using a centered leap-frog numerical scheme which is 2nd order in the horizontal and 4th order in the vertical. A detailed derivation of the 6-hour time-averaged form of *Advection* and a discussion of the numerical integration technique are given in section 3. of Mahlman and Moxim [1978].

The principal difficulty in simulating atmospheric transport lies in the numerical treatment of those atmospheric processes that are not resolved by, in our case, a 265 km grid: details of cyclones, fronts, squall lines, convection, and turbulence on a wide range of scales. All these subgrid-scale processes must be represented by parameterizations based on the resolved grid-scale variables. In all cases, including this study, the parameterizations are very crude physical representations of the actual physical process. This is particularly true of our treatment of vertical subgrid-scale transport by convective clouds. Using a diffusive closure, which is a product of the local tracer gradient and a diffusion coefficient, we attempt to capture the ensemble average of such processes, if not the individual detail, with a subgrid-scale tracer transport that is down-gradient. However, our diffusion coefficients are much more than simple constants and depend on properties of the local winds and local gradients of the tracer field.

Horizontal *Diffusion* employs a highly scale-selective diffusion coefficient,  $K_H$ , that follows from the formulation first introduced by Smagorinsky [1963].  $K_H$  is constructed so that, at the limit of very low horizontal-variability in the tracer field, the coefficient is 1/2 of the value used by the parent GCM, while in the limit of very high horizontal-variability, it is 10 times that value. This formulation was first developed and tested for a study of nuclear test debris, a high variability case, and for a study of tropospheric  $N_2O$ , a very low variability case. A detailed derivation and discussion of  $K_H$  is given in section 3. of Mahlman and

Moxim [1978] and in appendix A.2 of Levy et al. [1982].

There are two coefficients for vertical *Diffusion*, both of which are proportional to the square of a mixing length and to the vertical wind shear. The first coefficient,  $K_{vcon}$ , acts throughout the vertical column, has a constant mixing length of 30 m, and represents subgrid-scale vertical transport by moist and dry convective processes. It is activated only when the moist bulk Richardson number, as defined in equation A5 of Levy et al. [1982], is less than a specified critical value, which is meant to represent the onset of turbulence. A small additional term that depends on the tracer's vertical gradient is also included to reduce  $2\Delta z$  fluctuations. The derivation and a detailed discussion of  $K_{vcon}$  are given in appendix A.3 of Levy et al. [1982].

Finding that the transport model underestimates vertical mixing in the boundary layer, under conditions of large-scale stability when  $K_{vcon}$  is shut off, we have included an additional vertical shear-dependent coefficient,  $K_{vbl}$ , in the lowest three levels. Its form is

$$K_{vbl} = A \cdot L(z) 2 \left| \frac{\partial \vec{V}}{\partial z} \right| \quad (2)$$

where  $L(z)$  are the same height-dependent mixing lengths used by the parent GCM,  $\frac{\partial \vec{V}}{\partial z}$  is the vertical wind shear, and  $A$  is a scaling parameter that was 1.0 for the GCM and, based on observed tracer profiles, has been set to 0.5 for these transport studies. Further details are provided in section 2.1 of Levy and Moxim [1989] and section 2. of Kasibhatla et al., [1992].

*Filling* explicitly corrects negative mixing ratios, which are generally produced upstream of sharp gradients by numerical advection error. This model utilizes an essentially diffusive downstream borrowing approach, as explained in Mahlman and Moxim [1978].

*Sink<sub>dry</sub>*, the deposition of gas molecules and aerosols on soil, water, ice, snow and vegetation at the earth's surface, is represented by

$$Sink_{dry} = \frac{w_d(i)}{\Delta z} \cdot R_{11}(i) \left[ \frac{1}{[1 + w_d(i) / (C_d |\vec{V}_{eff}|)]} \right] \quad (3)$$

The term in the large brackets, which assumes a balance between surface deposition and the turbulent flux of the trace species in the bottom half of the lowest model level, reduces the mixing ratio in the lowest model level to its value at the earth's surface.  $w_d(i)$  is the measured deposition velocity for the  $i^{\text{th}}$  species,  $R_{11}(i)$  is its mixing ratio in the lowest model level,  $\Delta z$  is the thickness of that bottom level,  $C_d$  is the GCM's globally averaged surface drag coefficient [0.002], and  $|\vec{V}_{eff}|$  is the model's effective surface wind speed [for details, see section 2.4 in Levy and Moxim, 1989]. Over the ocean,  $w_d$  is 0.3 cm/s for  $\text{HNO}_3$  and 0.0 for PAN and  $\text{NO}_x$ . It is 0.5 cm/s for  $\text{HNO}_3$  and 0.0 for the other two over ice and snow. Over land, when the temperature in the lowest level,  $T_{11}$ , is  $>10^\circ \text{C}$ ,  $w_d$  is 1.5 cm/s for  $\text{HNO}_3$  and

0.25 cm/s for PAN and  $\text{NO}_x$ .  $T_{11} < -10^\circ \text{C}$  over land is treated the same as ice and snow. For temperatures between  $10^\circ \text{C}$  and  $-10^\circ \text{C}$  over land, the  $w_d$  values are linearly interpolated between the two land values mentioned above.

$Sink_{wet}$  is the deposition of soluble gases and aerosols in precipitation. We need only consider the highly soluble tracer  $\text{HNO}_3$  for this study. The wet removal scheme we use distinguishes between stable or shallow convective and deep convective precipitation. The fraction of  $\text{HNO}_3$  removed from the grid box is a function of the local precipitation rate, and the wet removal tendency is proportional to the local tracer mixing ratio (see section 2. in Kasibhatla et al. [1991] for details).

*Sources* consist of anthropogenic emissions of  $\text{NO}_x$  from fossil fuel combustion (21.3 tgN/yr) and biomass burning (8.5 tgN/yr) and natural or primarily natural sources, biogenic emissions from soil (7.5 tgN/yr), injection of stratospheric  $\text{NO}_x$  (0.6 tgN/yr) and lightning discharge (3-5 tg/yr).

The construction of the gridded fossil-fuel *Source* data base for  $\text{NO}_x$  is described in section 2.2 and the global distribution is given in Figure 1 of Levy and Moxim (1989). Detailed emission inventories from the U.S., Canada (7.5 tgN/yr) and Western Europe (5.9 tgN/yr) are supplemented with global estimates by Hameed and Dignon [1988] that are based on UN fuel use statistics. In the GCTM, the emissions, which are assumed to be constant throughout the year, are partitioned into a surface flux and volume sources in the bottom two model levels. We have added 0.015 tgN/yr of  $\text{NO}_x$  emissions from Prudhoe Bay [Jaffe et al., 1991] for this study. However, commercial aircraft, which emit  $\sim 0.5$  tgN/yr of  $\text{NO}_x$  to the free troposphere of the northern latitudes [Beck et al., 1992], are not included. While much smaller than the other anthropogenic sources, this direct emission into the free troposphere may have a significant impact, as is discussed by Ehhalt et al. in this proceeding

The global biomass burning *Source* of 8.5 tgN/yr, (see Figure 43.1 in Levy et al. [1991]), is emitted as a surface flux. It is constructed from a gridded [ $1^\circ$  latitude  $\times$   $1^\circ$  longitude] CO biomass burning source developed by Logan [private communication, 1990] and measured (field and laboratory) emission ratios for  $\text{NO}_x/\text{CO}_2$  and  $\text{CO}/\text{CO}_2$  [Andrea et al., 1988; Hao et al., 1989]. The burning period for each gridbox in the model between  $35^\circ \text{N}$  and  $35^\circ \text{S}$ , primarily the tropical rainforests and subtropical savannas of Africa and South America, is based on the precipitation data from the parent GCM. The driest three contiguous months are designated as the main burning period and 25% of the emissions is released in each month. The balance is emitted equally in the month preceding and the month following the burning period. Emissions only occur when precipitation is less than 0.01 inch/day. Poleward of  $35^\circ$ , the emissions from agricultural burning and forest fires are released during the summer months.

The Soil biogenic emissions *Source* (7.5 tgN/yr), which is sensitive to both soil temperature and nitrate level, is predominately from the subtropical savannas (3.2 tgN/yr) and the intensive agriculture regions of the mid-latitudes (2.8 tgN/yr) and should be considered both natural and anthropogenic. Net NO<sub>x</sub> emissions above the forest canopy are relatively low and NO<sub>x</sub> emissions from the tundra and taiga woodland of the North are extremely low, even during the summer [Bakwin et al., 1992]. Further details of the source are under preparation.

We use zonally and monthly averaged O<sub>3</sub> and N<sub>2</sub>O fields to calculate the production of NO in the stratosphere from the oxidation of N<sub>2</sub>O by O(1D) (see Kasibhatla et al. [1991] for details), and find a maximum rate of 200-240 molecule/cm<sup>3</sup>/s. The zonal distribution of the annual-average *Source* is shown in Figure 2 of Kasibhatla et al. [1991]. While NO<sub>x</sub> is produced continuously in the stratosphere, it is only injected episodically into the troposphere, particularly during the winter and spring at mid- and high latitudes. While this small source has a significant impact on NO<sub>y</sub> levels in the mid- and upper troposphere, it is predominately HNO<sub>3</sub> and has very little impact on NO<sub>x</sub> and PAN levels.

Lightning, which has been observed primarily over land in the tropics and subtropics [Orville and Spencer, 1979; Turman and Edgar, 1982], is an important *Source* of NO<sub>x</sub> in the free troposphere, particularly away from regions with strong surface sources. While estimates of the global source have ranged from 1-100 tgN/yr (see Logan [1983] and Liaw, et al. [1990] for detailed discussions), 20 tgN/yr is the upper limit permitted by known rates of nitrate deposition in remote regions [Logan, 1983]. However, due to lower OH and weaker deposition, the effective atmospheric lifetime for NO<sub>x</sub> emitted by lightning in the free troposphere is much longer than that for NO<sub>x</sub> emitted at the surface. Therefore, a few tgN/yr of lightning will have a major impact on the level of NO<sub>x</sub> and NO<sub>y</sub> in much of the free troposphere. Our lightning source is based on the incidence of deep moist convection in the parent GCM, with convection over the ocean weighted by 0.1 because lightning is much less frequent in maritime deep convection [Price and Rind, 1992]. The latitudinal distribution of our lightning source compares well with the observed yearly averaged lightning flash distributions of Turman and Edgar [1982] and Orville and Spencer [1979]. The vertical distribution of the source is based on the distribution of the height of flash origin and the ratio of cloud-cloud to cloud-ground lightning strokes from the study by Proctor [1991]. We assume that cloud-ground flashes produce 10 times as much NO<sub>x</sub> and use upper tropospheric observations of NO<sub>x</sub> near Dakar, Senegal [Drummond et al., 1988], NO<sub>y</sub> over the eastern Pacific during the NASA/CITE mission [Ridley, 1991], and NO<sub>y</sub> near Darwin, Australia [Murphy et al., 1992] to bracket the lightning source between 3-5 tgN/yr. We use 3 tgN/yr in this study.

*Chemistry*, involves the chemical interconversion of  $\text{NO}_x$ ,  $\text{HNO}_3$ , and PAN. The gas phase scheme described in section 3 and the appendix in Kasibhatla et al. (1991) is used for all sources, excepting fossil fuel combustion. In that case we use a standard  $\text{O}_3$ -CO- $\text{CH}_4$ - $\text{NO}_x$ - $\text{H}_x\text{O}_y$  chemical scheme [e.g. Chameides and Tans, 1981]. Hemispheric-average 1-D profiles of CO and  $\text{NO}_x$  and 2-D fields of  $\text{CH}_4$ ,  $\text{O}_3$ ,  $\text{H}_2\text{O}$ , T, p and total column ozone are specified from either available observations or GCM data (see the appendix in Kasibhatla et al. [1991] for details). The chemical production and loss terms for the 3 transported species are then calculated off-line and carried in the model as monthly 2-D tables. The following modifications have been made since Kasibhatla et al. [1991]: The night-time conversion of  $\text{NO}_x$  to  $\text{HNO}_3$ , by the reaction of  $\text{NO}_2$  with  $\text{O}_3$ , followed by the reaction of  $\text{NO}_3$  with  $\text{NO}_2$ , is included in the bottom two model levels; The ethane and propane fields needed for PAC (the PAN precursor) formation are now taken from the 2-D simulation of Kanakidou et al. [1991];  $\text{HO}_2$  and  $\text{RO}_2$  reactions are included in the calculation of  $\text{NO}/\text{NO}_2$ ; The new  $\text{OH} + \text{CH}_4$  reaction rate has been used [Vaghjiani and Ravishankara, 1991]. The resulting 2-D OH fields give a global  $\text{CH}_3\text{CCl}_3$  lifetime of ~6.2 years and are in reasonable agreement with more detailed calculations [e.g. Spivakovsky et al., 1990].

## RESULTS

The January average PAN distribution at the lowest model level [990 mb or ~80 m] is given in Figure 1. With mixing ratios of ~300 pptv, this  $\text{NO}_x$  reservoir specie is the major reactive nitrogen compound, both at the surface and in the free troposphere. PAN accumulates throughout the winter in the North, because it is extremely stable and unreactive in cold air and is not removed by surface deposition to ice, snow and frozen vegetation. Its mixing ratio remains relatively uniform from the ground to the upper troposphere and grows to a maximum of ~500 pptv in the spring. As the atmosphere and surface warm up in the summer months, PAN levels, away from local sources, drop to ~50 pptv at the surface and to 100-200 pptv in the free troposphere. While its mixing ratio is significantly lower in the summer, PAN remains relatively uniform and the dominant reactive nitrogen specie in the free troposphere. The January  $\text{NO}_x$  mixing ratios shown in Figure 2 are much more variable than those of PAN. Near source regions,  $\text{NO}_x$  levels exceed 1ppbv, while in the remote far north they drop to less than 100 pptv. In the free troposphere they range from 100 - 300 pptv and are comparable to PAN. However, unlike PAN,  $\text{NO}_x$  levels, away from local sources, reach a maximum in January and decrease steadily until the next fall when the rate of chemical conversion of  $\text{NO}_x$  to PAN and  $\text{HNO}_3$  again starts to decrease. In the summer,  $\text{NO}_x$  levels drop to less than 50 pptv throughout much of the northern troposphere. The one exception is in the boundary

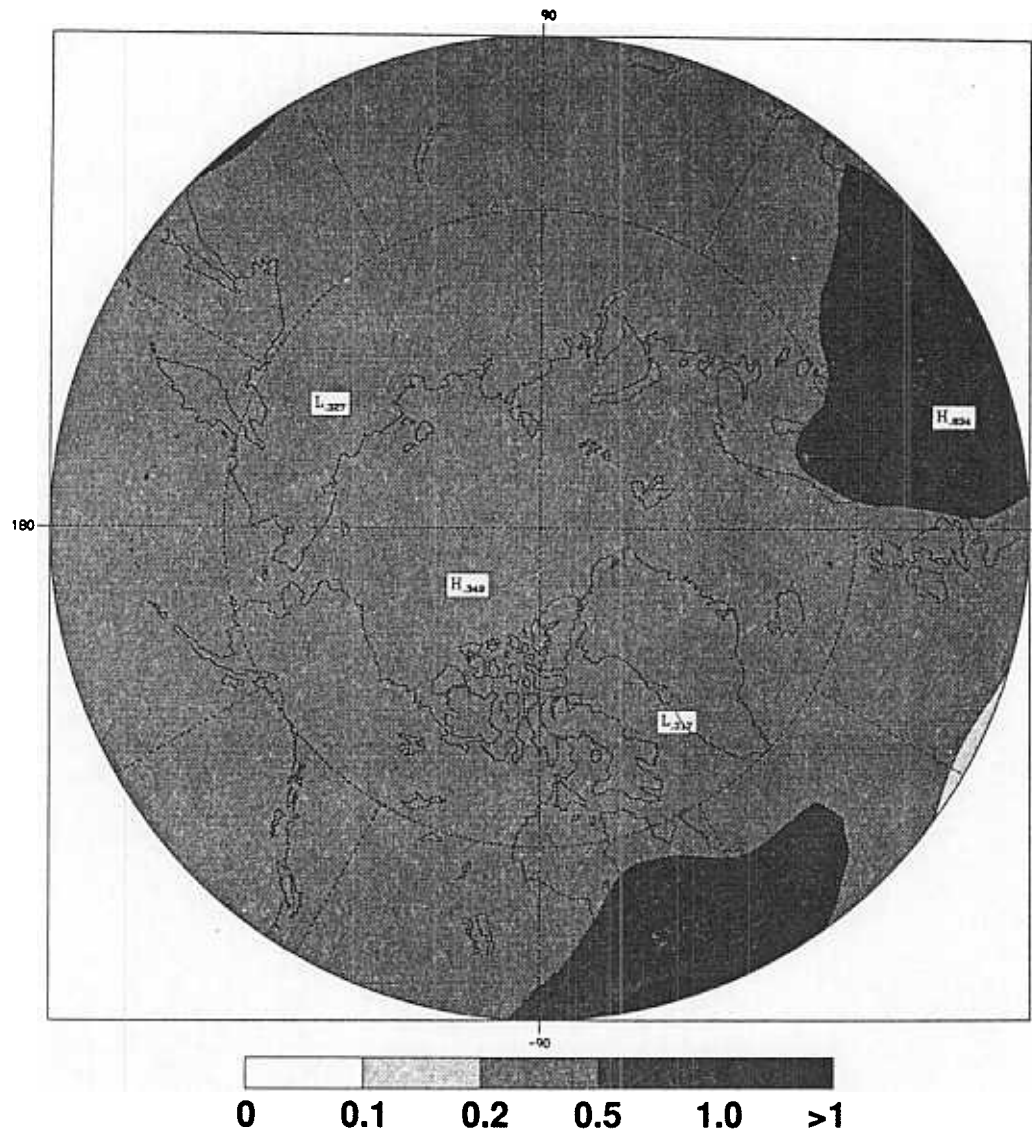


Figure 1. January monthly-average PAN mixing ratios [ppbv] in the lowest model level

layer near local sources such as biomass burning, soil biogenic activity and fossil fuel combustion. In this case,  $\text{NO}_x$  levels easily exceed 200 pptv and even reach 1 -10 ppbv in some polluted areas.

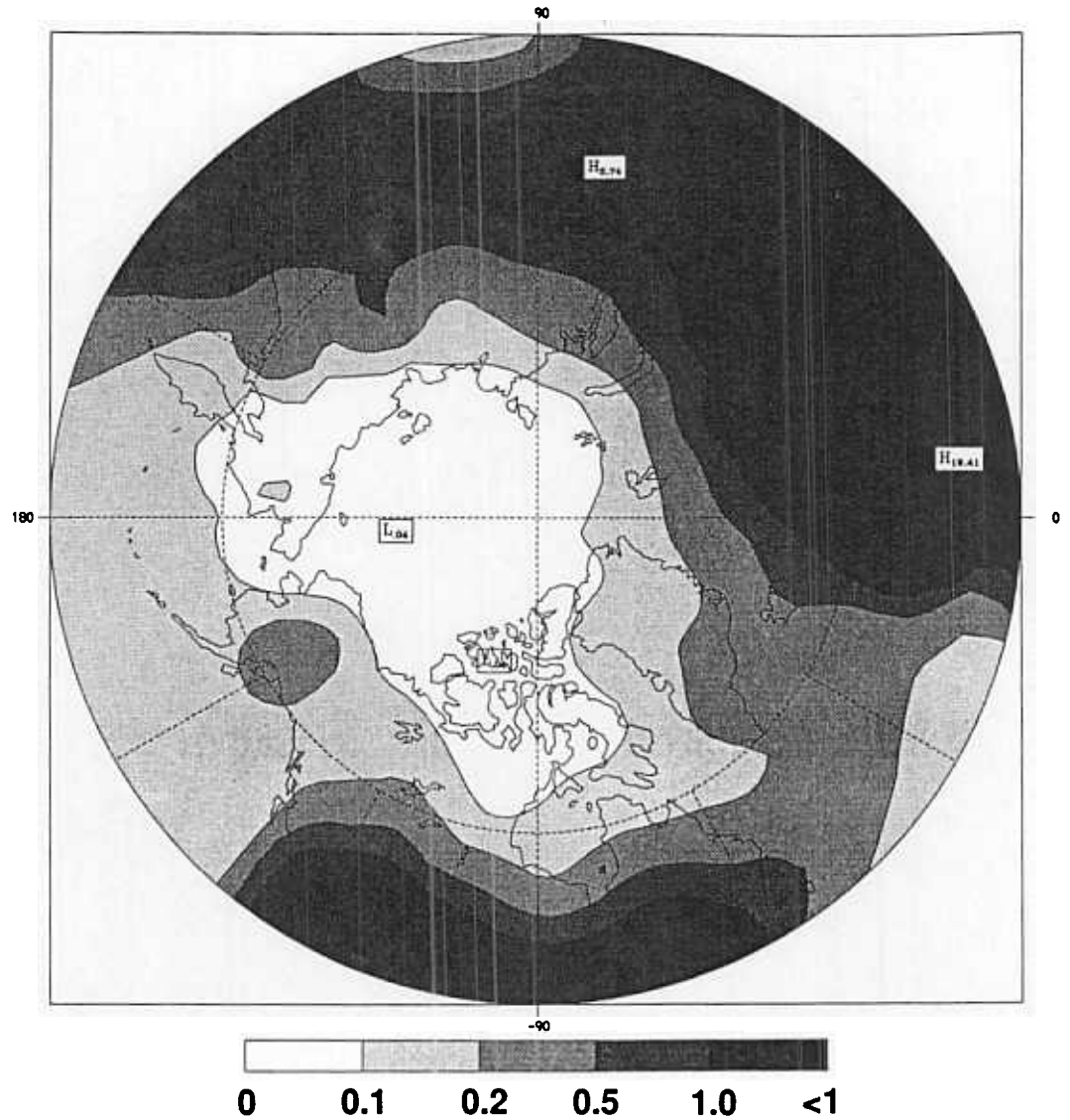


Figure 2. January monthly-average  $\text{NO}_x$  mixing ratios [ppbv] in the lowest model level

Before continuing with further analysis of the numerical simulation, it is instructive to compare the model simulations with available observations. It is difficult to compare short-term observations for a particular meteorological event with the simulations from a GCTM, which creates climatic statistics. Time-average values, particularly from multiple-year time-series, are best. In Table 1, we compare data from the lowest model level with two relatively

lengthy sets of surface observations: 1) A multiple year record of PAN (pptv) at Alert in Arctic Canada (82° N, 62° W) [Barrie and Bottenheim, 1991]; and 2) A 10 month record of NO<sub>y</sub> (pptv) at Barrow, Alaska (71° N, 157° W) [Honrath and Jaffe, 1992]. It would appear from the comparison in Table 1 that the model captures both the magnitude and the seasonal cycle of NO<sub>y</sub> and its major specie, PAN, in the Arctic boundary layer. At this time,

Table 1: Surface Mixing Ratio (pptv) Measurements and Model Results in the Arctic

	Winter		Spring		Summer		Fall	
	obs.	model	obs.	model	obs.	model	obs.	model
Alert								
PAN	150-250	350	250-500	490	<50	35	75-100	130
Barrow								
NO <sub>y</sub>			500-700	530	50-100	50-75	100-200	130
NO <sub>x</sub>					15-50*	15-30		

\* Only NO was measured. NO<sub>x</sub> was calculated.

while the expected long lifetime of PAN and a few spot measurements support the model's prediction that PAN is the principal reactive nitrogen specie throughout the free troposphere, conclusive confirmation is not yet available.

Given the fact that NO<sub>x</sub> emissions from lightning, biogenic emissions and biomass burning primarily occur in the summer, it should come as no surprise that fossil fuel emissions are the overwhelming source of NO<sub>x</sub> and PAN throughout the winter and spring in the northern latitudes. From our GCTM simulations, we find that 85 to 90% of the winter and spring storage comes from fossil fuel emissions. In the summer, other sources become important, and the contribution from fossil fuel combustion drops to ~50%. For the final study, which considers the potential impact of the stored PAN and NO<sub>x</sub> on springtime NO<sub>x</sub> levels in the northern latitudes, we will focus on fossil fuel combustion only.

While the GCTM predicts, as previous observations have suggested, that high levels of PAN and NO<sub>x</sub> are stored throughout the winter in the northern latitudes, the relative importance of such storage, when compared with ongoing NO<sub>x</sub> emissions, has never been quantified. Integrating the NO<sub>x</sub> and PAN fields from 40° N to the Pole and from the ~900 mb

to ~240 mb, which excludes the boundary layer emission region, we find that 0.07 tgN of each are stored in January. The integral of stored PAN in the region increases to ~0.11 tgN by March, while NO<sub>x</sub> drops to 0.025 tgN. The total amount of NO<sub>x</sub> and PAN, itself a potential indirect source of NO<sub>x</sub>, stored in the northern latitudes during the winter and early spring is ~0.14 tgN, and it can be compared to the monthly midlatitude emissions from fossil fuel combustion in the boundary layer (~1.5 tgN) and from commercial aircraft in the free troposphere (~0.05 tgN). While the PAN and NO<sub>x</sub> stored at high latitudes are potentially important sources of NO<sub>x</sub> at midlatitude during the springtime onset of ozone photochemistry, the levels are of the same order as direct emissions into the free troposphere by aircraft and only 0.1 of the surface emissions from fossil fuel combustion. A quantitative examination of the impact of stored PAN and NO<sub>x</sub> on springtime NO<sub>x</sub> levels and of the relative roles of PAN chemistry and atmospheric transport is now in progress and will be discussed in a later paper.

## REFERENCES

- Andrea, M.O., et al., Biomass-burning emissions and associated haze layers over Amazonia, *J. Geophys. Res.*, *93*, 1509 - 1527, 1988.
- Bakwin, P. S., et al., Reactive nitrogen oxides and ozone above a taiga woodland, submitted to *J. Geophys. Res.*, 1992.
- Barrie, L. A. and J. W. Bottenheim, Sulfur and nitrogen pollution in the Arctic atmosphere, in: *Pollution of the arctic atmosphere*, W.T. Sturges, Editor, p.155-183, Elsevier Science Publishers, London, 1991.
- Beck, J. P., C. E. Reeves, F. A. A. M. de Leeuw, and S. A. Penkett, The effect of aircraft emissions on tropospheric ozone in the northern hemisphere, *Atmos. Environ.*, *26A*, 17 - 29, 1992.
- Chameides, W. L. and A. Tans, The two-dimensional diagnostic model for tropospheric OH: An uncertainty analysis, *J. Geophys. Res.*, *86*, 5209-5223, 1981.
- Drummond, J. W., D. H. Ehhalt, and A. Volz, Measurements of nitric oxide between 0-12 km altitude and 67° N to 60° S latitude obtained during STRATOZ III, *J. Geophys. Res.*, *93*, 15831-15849, 1988.
- Hao, W. M., M. H. Liu, and P. J. Crutzen, Estimates of annual and regional releases of CO<sub>2</sub> and other trace gases to the atmosphere from fires in the tropics, based on FAO statistics from the period 1975 - 1980, *Presented at Third International Symposium on Fire Ecology*, Freiburg University, Federal Republic of Germany, 1989.
- Hameed, S. and J. Dignon, Changes in the geographical distributions of global emissions of NO<sub>x</sub> and SO<sub>x</sub> from fossil fuel combustion between 1966 and 1980, *Atmos. Environ.*, *22*, 441-449, 1988.

- Honrath, R. E. and D. A. Jaffe, The seasonal cycle of nitrogen oxides in the Arctic troposphere at Barrow, Alaska, *J. Geophys. Res.*, *in press*, 1992.
- Jaffe, D. A., R. E. Honrath, J. A. Herring, S.-M. Li, and J. D. Kahl, Measurements of nitrogen oxides at Barrow, Alaska during spring: Evidence for regional and Northern Hemisphere sources of pollution, *J. Geophys. Res.*, *96*, 7395-7405, 1991.
- Kanakidou, M., H. B. Singh, K. M. Valentin and P. J. Crutzen, A two-dimensional study of ethane and propane oxidation in the troposphere, *J. Geophys. Res.*, *96*, 15395-15425, 1991.
- Kasibhatla, P. S., H. Levy II, W. J. Moxim, and W. L. Chameides, The relative impact of stratospheric photochemical production on tropospheric NO<sub>y</sub> levels: A model study, *J. Geophys. Res.*, *96*, 18631 - 18646, 1991.
- Kasibhatla, P. S., H. Levy II, and W. J. Moxim, Global NO<sub>x</sub>, HNO<sub>3</sub>, PAN and NO<sub>y</sub> distributions from fossil-fuel combustion emissions: A model study, *J. Geophys. Res.*, *submitted*, 1992.
- Liaw, Y., D. L. Sisterson and N. L. Miller, Comparison of field, laboratory, and theoretical estimates of global nitrogen fixation by lightning, *J. Geophys. Res.*, *95*, 22489-22494, 1990.
- Levy II, H., J. D. Mahlman, and W. J. Moxim, Tropospheric N<sub>2</sub>O variability, *J. Geophys. Res.*, *87*, 3061 - 3080, 1982.
- Levy II, H., and W. J. Moxim, Simulated global distribution and deposition of reactive nitrogen emitted by fossil fuel combustion, *Tellus*, *41*, 256 - 271, 1989.
- Levy II, H., W. J. Moxim, P. S. Kasibhatla, and J. A. Logan, The global impact of biomass burning on tropospheric reactive nitrogen, in: *Global biomass burning: Atmospheric, climatic, and biospheric implications*, J.S. Levine, Editor, p. 363-369, MIT Press, Cambridge, Mass., 1991.
- Logan, J. A., Nitrogen oxides in the troposphere: Global and regional budgets, *J. Geophys. Res.*, *88*, 10785 - 10807, 1983.
- Mahlman, J. D., and W. J. Moxim, Tracer simulation using a global general circulation model: Results from a midlatitude instantaneous source experiment, *J. Atmos. Sci.*, *35*, 1340 - 1374, 1978.
- Manabe, S., D. G. Hahn, and J. L. Holloway, Jr., The seasonal variation of the tropical circulation as simulated by a global model of the atmosphere, *J. Atmos. Sci.*, *31*, 43 - 83, 1974.
- Manabe, S., and J. L. Holloway, Jr., The seasonal variation of the hydrologic cycle as simulated by a global model of the atmosphere, *J. Geophys. Res.*, *80*, 1617 - 1649, 1975.

- Murphy, D. M., D. W. Fahey, S. C. Liu, M. H. Proffitt, and C. S. Eubank, Measurements of reactive odd nitrogen and ozone in the upper troposphere and lower stratosphere, *J. Geophys. Res.*, *in press*, 1992.
- Orville, R. E. and Spencer D. W., Global lightning flash frequency, *Mon. Weather Rev.*, *107*, 934, 1979.
- Price, C. and D. Rind, A simple lightning parameterization for calculating global lightning distributions, *J. Geophys. Res.*, *97*, 9919-9934, 1992.
- Proctor, D. E., Regions where lightning flashes began, *J. Geophys. Res.*, *96*, 5099 - 5112, 1991.
- Ridley, B. A., Recent measurements of oxidized nitrogen compounds in the troposphere, *Atmos. Environ.*, *25A*, 1905 - 1926, 1991.
- Singh, H. B., L. J. Salas and W. Viezee, Global distribution of peroxyacetyl nitrate, *Nature*, *321*, 588-591, 1986.
- Smagorinsky, J., General circulation experiments with the primitive equations. I. The basic experiment, *Mon. Wea. Rev.*, *91*, 99-164, 1963.
- Spivakovsky, C. M., S. C. Wofsy, and M. J. Prather, A numerical method for parameterization of atmospheric chemistry: Computation of tropospheric OH, *J. Geophys. Res.*, *95*, 18433-18440, 1990.
- Turman, B. N. and Edgar, B. C., Global lightning distribution at dawn and dusk, *J. Geophys. Res.*, *87*, 1191-1206, 1982.
- Vaghjiani, G. L. and A. R. Ravishankara, New measurements of the rate coefficient for the reaction of OH with methane, *Nature*, *350*, 406-409, 1991.